Pd-Cu-M (M= Y, Ti, Zr, V, Nb, and Ni) alloys for the hydrogen separation membrane

Nayebossadri, Shahrouz; Speight, John; Book, David

DOI:
10.1021/acsami.6b12752

Document Version
Peer reviewed version

Citation for published version (Harvard):
Nayebossadri, S, Speight, J & Book, D 2016, 'Pd-Cu-M (M= Y, Ti, Zr, V, Nb, and Ni) alloys for the hydrogen separation membrane', *ACS Applied Materials & Interfaces*, vol. 9, no. 3, pp. 2650-2661. https://doi.org/10.1021/acsami.6b12752

Article

Pd-Cu-M (M= Y, Ti, Zr, V, Nb, and Ni) alloys for hydrogen separation membrane

Shahrouz Nayebossadri, John D. Speight, and David Book

ACS Appl. Mater. Interfaces, **Just Accepted Manuscript** • DOI: 10.1021/acsami.6b12752 • Publication Date (Web): 19 Dec 2016

Pd-Cu-M (M= Y, Ti, Zr, V, Nb, and Ni) alloys for hydrogen separation membrane

Shahrouz Nayebossadri*, John D. Speight, David Book
School of Metallurgy and Materials, University of Birmingham,
Edgbaston, Birmingham, B15 2TT, UK
E-mail: s.nayebossadri@bham.ac.uk
Tel: (+44) (0) 121 414 5213

Abstract

Self–supported fcc Pd–Cu–M (M= Y, Ti, Zr, V, Nb, and Ni) alloys were studied as potential hydrogen purification membranes. The effects of small additions (1–2.6 at.%) of these elements on the structure, hydrogen solubility, diffusivity, and permeability were examined. Structural analyses by XRD showed fcc phase for all alloys with induced textures from cold rolling. Heat treatment at 650 °C for 96 h led to the re–orientation in all alloys except Pd–Cu–Zr alloy, exhibiting the possibility to enhance the structural stability by Zr addition. Hydrogen solubility was almost doubled in the ternary alloys containing Y and Zr compared to $Pd_{65.1}Cu_{34.9}$ alloy at 300 °C. It was noted that hydrogen diffusivity is decreased upon additions of these elements compared to $Pd_{65.1}Cu_{34.9}$ alloy, with Pd–Cu–Zr alloy showing the lowest hydrogen diffusivity. However, the comparable hydrogen permeability of Pd–Cu–Zr alloy with the corresponding binary alloy, as well as its highest hydrogen permeability amongst the studied ternary alloys at temperatures higher than 300 °C suggested that hydrogen permeation of these alloys within the fcc phase is mainly dominated by hydrogen solubility. Hydrogen flux variations of all ternary alloys were studied and compared with $Pd_{65.1}Cu_{34.9}$ alloy under 1000 ppm H_2S+H_2 feed gas. Pd–Cu–Zr alloy showed superior resistant to the sulphur poisoning probably due to the less favourable H_2S–surface interaction and more importantly slower rate of bulk sulfidation as a result of improved structural stability upon Zr addition. Therefore, Pd–Cu–Zr alloys may offer new potential hydrogen purification membranes with improved chemical stability and hydrogen permeation compared to the binary fcc Pd–Cu alloys.

Keywords: Hydrogen separation, Metallic membranes, Pd-based membranes, Pd-Cu,

Ternary alloys

1. Introduction

Amongst Metal-Hydrogen systems, palladium-hydrogen (Pd–H) system is one of the most extensivley studied system [1]. Hydrogen seperating membrane developed based on the dense palladium (Pd) metal offers excellent permeability for hydrogen as a result of the solution–diffusion mechanism [2]. Despite unique ability of palladium to permeate hydrogen, the use of the pure palladium membrane is hindered because the Pd–H system shows two distinct immiscible α (interstitial hydrogen solid solution at temperatures and pressures below 300 ºC and 2MPa) and β (palladium hydride) phases. Hydrogenation of Pd results in almost 10% increase in the lattice volume due to the phase transition. The volume increase inevitably creates high levels of stress leading to the structural distortion, deformation and finally membrane failure [2-4]. Furthermore, the metallic nature of pure Pd makes it susceptible to surface poisoning by impurity gases [5-7]. These problems, as well as the high cost of Pd have led to the exploration of a wide variety of Pd–alloy membranes [8-10].

Amongst these alloys, the lower cost and some tolerance to the surface poisoning as demonstrated by the face centered cubic (fcc) structure of palladium–copper (Pd–Cu thereafter) signifies the importance for further development of this alloy[11-19]. The permeability of Pd–Cu alloys is significantly depending on the Cu concentration and therefore the structure of the alloy[11, 20]. For example, the reported hydrogen permeability value for the $Pd_{47}Cu_{53}$ (at.%) alloy at 350 $^{\circ}$C [11] with a CsCl–type ordered bcc structure [20] exceeds than that of pure Pd. High hydrogen permeability in the bcc phase of the Pd–Cu alloy is attributed to almost two times faster hydrogen diffusion in the ordered bcc phase compared to the fcc phase of Pd–Cu alloy at ambient temperature. [11-12,15].

Nevertheless, hydrogen permeability in the bcc phase of the Pd–Cu alloy is highly sensitive to the gas impurities. It was shown that whilst $Pd_{47}Cu_{53}$ alloy could easily become impermeable to hydrogen under 1000 ppm H_2S, an increase in the temperature could improve

the alloy's tolerance to the sulphur poisoning as a result of structural transition from bcc to fcc structure [19,21]. It was shown [22] that the complete suppression of hydrogen flux only takes 5 minutes after exposing the bcc $Pd_{47}Cu_{53}$ alloy to 1000 ppm H_2S at 350 ºC. The formation of Pd–Cu–S layer on the surface of the $Pd_{47}Cu_{53}$ alloy was confirmed by X-ray Photoelectron Spectroscopy (XPS) measurement which was suggested to be responsible for rapid decline in the hydrogen flux [22]. Hydrogen flux at various temperatures through Pd–Cu membranes was also studied when the membranes subjected to different H_2S concentrations [23]. Low H_2S concentrations were suggested to block the active surface sites required for hydrogen dissociation, hence reducing the hydrogen flux. However, H_2S concentrations of approximately 300 ppm at 450 ºC were shown to trigger the sulfidation process, lattice expansion and consequently permanent failure in the Pd–Cu membranes regardless of the exposure time.

$Pd_{70}Cu_{30}$ thin film (~2μm) were also exposed to various H_2S concentrations of 2, 20 and 100 ppm at 450 ºC and hydrogen flux was substantially reduced in all cases[24]. The hydrogen flux recovery tests showed that after removal of 2 ppm H_2S the hydrogen flux could be fully recovered to its original value within 2 h. however, only 95 % of the original hydrogen flux value was recovered within 2–3 h and 24 h after removal of 20 and 100 ppm H_2S respectively [24]. Iyoha et al.[25] experimentally investigated sulfidation of $Pd_{70}Cu_{30}$ alloy at different H_2S to H_2 partial pressures and validated their thermodynamic calculations indicating the required H_2S concentration for the formation of Pd_4S and Cu_2S sulphides within a temperature range of 77 to 977 ºC in this alloy. However, SEM and EDS analyses revealed extensive Cu segregation at the surface of Pd–Cu alloys, altering the surface chemical composition, and leading to the formation of non–ideal solid solution in Pd–Cu alloys. Hence, some deviation in the calculated thermodynamic values required for the sulfidation of Pd–Cu alloys was observed. It has been shown [5] that surface segregation can be

encouraged when the metallic membrane is interacting with the gas species with a high tendency for surface adsorption, *e.g.* sulphur. Consequently, sulfidation may promote surface segregation of some particular elements in the alloy and irreversibly altering the surface structure, surface chemical composition and eventually ceasing hydrogen permeation through the membrane[26]. Nevertheless, controlled surface segregation of the alloying elements can be useful to alleviate sulfidation. For instance, Pd–Au membranes show a higher resistant to the sulphur poisoning when compared to the other Pd–based membranes [6,27,28]. It is suggested that a high Au tendency for surface segregation causes a higher Au concentration on the alloy's surface, leading to an increased sulphur tolerance [29,30]. This promotes the formation of dilute Pd structures less favourable for sulphide phase formation in agreement with the theoretical study indicating that H_2S dissociation is much less favourable on Au rich surfaces [6,31].

In addition, the membrane fabrication method seems to influence the membrane stability in H_2S containing atmosphere. It was shown that [23] electroless–platted Pd–Cu membranes fail at much lower H_2S concentrations when compared to the same cast and rolled membrane. This was attributed to the higher sticking coefficient of sulphur on the rougher surfaces as a result of greater surface area, more intrinsic stress and less uniform alloy composition of thin films compared to the cast and rolled foils. The effect of fabrication method was also investigated by Gade *et al.* [27] on the stability of a series of sputtered and cold rolled Pd–Au membranes in H_2S containing atmosphere. Membrane produced by magnetron sputtering underwent an irreversible loss of selectivity but cold worked membranes retained acceptable selectivity. This was related to the pattern of the grain boundaries which were perpendicular to the surface, hence conducting sulphur more deeply into the bulk. The thickness of the sputtered membrane was significantly decreased as a result

of palladium sulphide flake off the feed surface, a process which happened to a less extent for the cold worked samples.

Ternary Pd–Cu–M alloys (M: metallic element) have been theoretically [32-34] and experimentally [35-40] studied in order to improve the hydrogen permeability and thermal stability. Hydrogen permeability showed to be improved after addition of some selected metallic elements. However, the effects of these metallic elements were not necessarily similar and even could be opposing on the hydrogen solubility and diffusivity of the alloy. Recently, we also investigated [40] structure and hydrogen permeability of Pd–Cu alloys after addition of a small amount of Ag. Whilst Ag addition always resulted in a lower diffusion coefficient, it could always increase hydrogen solubility in the Pd–Cu–Ag samples compared to Pd–Cu alloys. Effects of the Ag additions on the hydrogen permeability of Pd–Cu–Ag alloys with bcc and (bcc+fcc) structures were investigated. It was proposed, that is the hydrogen diffusion which mostly controls hydrogen permeability in the bcc phase and therefore an enhancement in solubility may be only beneficial in improving hydrogen permeability when the fcc phase exists.

It seems that the general approach to increase the hydrogen flux and reduce the cost of the fcc Pd–Cu alloys is through fabrication of ternary Pd–Cu thin film alloys. However, the desired resistance to surface poisoning needs to be maintained and fortified in the case of Pd–Cu thin films. A possible method may be adding elements, which show a preferential segregation leading to a less S–surface interaction. However, preferential segregation may be detrimental to the long term stability requirement of the membrane, causing degradation in the membrane properties similar to the flake off problem observed for Au addition [27]. Hence, in this study we try to stabilise the alloy structure in order to minimise the segregation and possibly alleviating the interaction between alloy and sulphur. The effects of selected additional elements on the hydrogen solubility, diffusivity, and permeability of the fcc Pd–

Cu–M (M= Y, Ti, Zr, V, Nb, and Ni) alloys are investigated. In addition, the performance of these alloys under the hydrogen feed gas atmosphere containing 1000 ppm H_2S are monitored and possible effects of additional elements are discussed.

2. Materials and method

The starting elements, palladium powder with a purity of 99.9985% and copper wire (1mm in diameter) with a purity of 99.9% were purchased from Alfa Aesar and Sigma Aldrich respectively. Pd–Cu alloy buttons with fcc structure (each weighing approximately 2.5 g) were prepared by arc melting after loading into a water–cooled copper hearth. A rotary pump was used to create a vacuum (approximately 10^{-2} mbar) which was then flushed with argon three times before being filled with 0.8 bar of argon. The Pd–Cu alloy buttons were turned into the foils by cold rolling and then additional elements (Y, Ti, Zr, V, Nb, and Ni) were deposited on the foils surface using a Closed Field Unbalanced Magnetron Sputter Ion Plating (CFUBMSIP) system supplied by Teer Coatings Ltd. The sputtering chamber was evacuated to approximately 10^{-6} mbar and refilled with ultra–high purity argon prior to the deposition. The target to substrate distance was kept constant and a sample rotation of 5 rpm was selected. Concentrations of the additional elements were calculated from the weight gain of the samples. Samples were re-melted for 3 times and then cold rolled to foils with the aimed thickness of 100 microns. The rolled alloys were heat treated at 650 °C for 96 h under vacuum (10^{-5} mbar) to ensure the homogeneity of the membranes.

Structural analysis were performed by a Bruker D8–Advanced diffractometer using monochromatic CuKα radiation (λ = 1.54056 Å). Temperature dependence structural analysis was performed using an Anton Parr XRK900 high–temperature sample cell. Structural evolutions of alloys were monitored under 5 bar flowing hydrogen (100 ml/min) and a heating rate of 2 $^{\circ}$C min^{-1}. JEOL 6060 Scanning Electron Microscopy (SEM) equipped with

an INCA 300 Energy Dispersive Spectroscopy (EDS) was used for compositional analysis and thickness measurements.

Hydrogen flux was measured through membrane disks, cut off from the rolled foils with an area of 2.54 cm^2. Membrane disks were cleaned in acetone and mounted in the hydrogen permeation system designed and built in the authors group [41]. Membranes sealed between a knife-edge and an annealed copper gasket and a leak test was performed under 5 bar pressure differential using nitrogen gas (99.95%), supplied by BOC. The pressure increase in the downstream side of the membrane was monitored by a pressure transducer with an accuracy of ±0.25%. All samples were gas tight before starting the experimental work as no pressure increase was observed in the downstream side of the membrane after at least 2 h. The system was de-gassed under 10^{-5} mbar vacuum prior to hydrogen (99.99995%, BOC) admittance. The feed gas was controlled using Brooks 5850S Mass Flow Controller (MFC) calibrated over a range of 6–600 ml min^{-1} with an accuracy of ±6 ml min^{-1}. Another Brooks 5850S MFC was used on the bleed side ensuring continuous hydrogen flow on the upstream side of the membrane. A constant hydrogen pressure of 6.18 was used on the upstream side and the downstream pressure was maintained at 1 bat during hydrogen permeation measurements using a back pressure regulator followed by a Brooks 5850S MFC to measure the permeated gas flow. The membranes temperatures as well as upstream and downstream temperatures were increased by a heating rate of 2 $^{\circ}C$ min^{-1} using an Elite Thermal Systems Ltd. split furnace. The stability of the membranes under gas streams containing H_2S were examined by switching the pure hydrogen feed (200 ml min^{-1}) to the 1000±10 ppm H_2S+H_2 gas mixture at 450 ºC purchased from BOC.

Hiden Isochema Intelligent Gravimetric Analyser (IGA) to measure hydrogen solubility in foils under a constant hydrogen pressure. The foils surfaces were lightly ground and washed in acetone before loading into the IGA. Samples with a weight of approximately

100±7 mg were loaded and subjected to the hydrogen pressures of 6.18 and 1 bar to resemble the condition used for hydrogen permeation measurements. The weight changes were recorded from room temperature to 450 °C hence, enabling to calculate H/M atomic ratios. H/M gradients through the thickness of membrane were determined by subtracting H/M atomic ratios calculated at 6.18 and 1 bar, similar to the procedure used elsewhere [42]. The above procedure has been repeated at least 4 times for each sample to ensure the reproducibility of results. Hydrogen concentration gradients were calculated knowing the H/M gradients, density, and the molecular weight of the alloys.

Fick's first law was used to calculate the hydrogen diffusion coefficients in the foils according to the following equation [42]:

$$J = D\,A\,\Delta c/\mathrm{x} \qquad (1)$$

Where J is hydrogen flux, D is diffusion constant, A is surface area of membrane, Δc hydrogen concentration gradient and x is the membrane thickness.

3. Results

3.1 Structural and compositional analyses

Fig. 1 (a–g) shows the XRD patterns of Pd–Cu and Pd–Cu–M alloys after fabrication and following vacuum heat treatment at 650 °C for 96 h. All the as–fabricated alloys demonstrate a relatively wide XRD patterns belonging to fcc structure. The structural similarity in all alloys after fabrication indicate that the presence of a small amount of additional elements do not encourage the formation of a new phase in Pd–Cu–M alloys. Whilst random orientation of grains in powdered Pd–Cu alloy results in a XRD pattern with a highest reflection intensity along (111) plan [38], a preferential orientation along the (220) plan can be observed for the as–fabricated Pd–Cu alloy in Fig. 1a, possibly due to the cold rolling process. Similar preferential orientation along the (220) plan can be observed in the XRD

patterns of the other Pd–Cu–M alloys after fabrication except the ones containing Nb and Y, where preferential orientations along the (111) plane seems to be dominated (Fig 1 b–g). The effects of the vacuum heat treatment at 650 ºC for 96 h on the structure of the same samples are shown in in Fig. 1 (h–n). The alloys initial fcc structure seems to remain intact after the heat treatment. However, the XRD patterns of the heat treated alloys become sharper possibly as a result of grain growth and stress relief. A small shoulder at higher 2θ values also seems to appear after annealing the Pd–Cu and ternary alloys containing Y, Nb and Ni probably as a result of compositional inhomogeneity on the top layer of these alloys due to the surface segregation of the alloying elements. Preferential orientations along (111) plane are observed for all the annealed samples, except ternary alloys containing V and Zr, indicating the thermal structural rearrangements of the samples by local atomic diffusion. Interestingly, whilst a new preferential orientation along (200) plan can be seen for Pd–Cu–V alloy (Fig. 1l), Pd–Cu–Zr alloy retains its structure and preferential orientation along the (220) plan (Fig. 1n) after annealing. This may refer to the structural stability of this alloy and minimal local atomic diffusion at the performed annealing condition.

Atomic compositions of the annealed samples were analysed by EDS, averaging various (at least three readings) area scans (>10^3 μm^2) of cross section and the results are listed in Table 1. No significant variations in the composition were observed across the alloys cross section indicating the homogeneity of the alloys (Table S1 in supporting information). EDS analyses further conforms the fcc structure of all alloys as observed by XRD in Fig. 1, giving elemental compositions in the fcc region of the Pd–Cu phase diagram [20]. The Pd atomic composition (x_{Pd}) in Pd–Cu alloys can be calculated from equation (2) by knowing the fcc lattice constant (a)[14,16]:

$$a_{fcc} = 0.36462 + (2.44 \times 10^{-4})\, x_{Pd} \qquad (2)$$

Using this method we have calculated the atomic composition for palladium in the Pd–Cu alloy to be x_{Pd}= 65.5 at%, which is very close to the value obtained by EDS analysis. However, it has been noted [40] that equation (2) is not applicable for the ternary Pd–Cu alloys as it overestimates the Pd content due to the lattice expansion induced by additional elements. Hence, in this work alloys compositions from EDS analyses are used to compare the properties and performance of the ternary alloys against each other and the Pd–Cu alloys with a same Pd content.

Effects of the additional elements on lattice size can be investigated by comparing lattice parameters of the Pd–Cu–M alloys with the previously reported [14,16,46-48] lattice parameters of Pd–Cu alloys plotted in Fig. 2 as a function of Pd concentration. The effectiveness of the Ag additions in expanding the lattice parameter of Pd–Cu–Ag alloys has been shown by theoretical calculation [34] and also experimentally confirmed [36,40]. It can be seen in Fig. 2 that the lattice parameter calculated for our Pd–Cu sample shows an excellent agreement with the reported values. Fig. 2 also shows that the lattice parameters of all ternary alloys are greater than the binary alloys with a same Pd content except Pd–Cu–Ni alloy, which shows almost a similar lattice parameter compared to the binary alloy. The highest lattice expansion of 0.31 % is observed by substituting small amounts of Cu for Y in the Pd–Cu–Y alloy. This is to be expected, because Y shows the biggest atomic size difference (1.80 Å) with Cu (1.35 Å), amongst the additional elements used in this study. Here, identical lattice parameter with the Pd–Cu alloy can be observed when Cu is replaced by Ni with a similar atomic radius. In contrast, the Pd–Cu–V sample shows a lattice expansion of almost 0.16 % compared to the binary alloy, despite the fact that V has a similar atomic radius to Cu. Although the variation in the lattice parameters of the Pd–Cu–M alloys may be mainly controlled by the atomic radius of the substitutional atoms for Cu, other factors may also contribute to the observed lattice expansions. Size factor anomalies have been reported in the

lattice parameters of some α phase Pd alloys [49]. It was noted that despite a very similar atomic radius for Th (Thorium) and Y, palladium lattice expanded to a larger extent upon Th addition [50]. This effect was attributed to the to the more rapid filling of vacant Pd 4d states by the tetravalent Th as compared to trivalent Y. Similarly, the higher lattice expansion observed in the case V may originate from its higher effective valence electron (Table 1) as compared to Ni.

3.2 Solubility and diffusivity

Hydrogen solubility gradients (ΔH/M atomic ratio) of the annealed binary and ternary alloys are shown as a function of temperature in Fig. 3a–g (Table S2 in supporting information for hydrogen solubility data points). A common feature of the curves is that they all show a small initial increase (maximum) in the range 20–50 °C and a subsequent sharp decrease in ΔH/M upon increasing the temperature to around 100 ºC. For all the alloys there are only small variations in ΔH/M from 100 to 450 °C, which hydrogen solubility values higher than 300 ºC mainly contribute to the hydrogen permeation (will be shown later). Pd–Cu alloys with more than 30 at% Cu effectively suppress the α to β phase transition at room temperature [46]. Hence, the reported hydrogen solubility values in Fig. 3 should relate to the dilute hydrogen solution, *i.e.* α phase. Fig. 3a shows a ΔH/M value of ~0.014 at room temperature for $Pd_{65.1}Cu_{34.9}$ sample, which is in a good agreement with the presently reported range for dilute hydrogen solution in Pd–Cu alloys [15, 51,52]. Whilst, the observed ΔH/M maximum at the beginning of heating process can be related to the improved hydrogen absorption kinetics and therefore hydrogen saturation in the Pd–Cu and Pd–Cu–M alloys, the subsequent sharp decrease observed between 50–100 ºC probably originates from an increase in the hydrogen absorption equilibrium pressure at higher temperatures. The ΔH/M value at 300 ºC for the $Pd_{65.1}Cu_{34.9}$ sample is less than half the value observed at room temperature

and shows small fluctuations by increasing temperature to 450 ºC. The effects of Ti and Nb additions (Fig. 3b–c) on the hydrogen solubility seem to be insignificant when compared to the $Pd_{65.1}Cu_{34.9}$ sample at 300 ºC. However, increasing temperature to 450 ºC leads to the lower ΔH/M values for ternary alloy containing Nb compared to the ternary alloy with Ti and $Pd_{65.1}Cu_{34.9}$ sample. Hydrogen solubility value for the ternary alloy with Ni in Fig. 3d is almost half the value observed for $Pd_{65.1}Cu_{34.9}$ sample at 300 ºC and remains constant upon increasing temperature to 450 ºC. In Pd–Cu alloys, an increase in the Cu concentration is expected to reduce hydrogen solubility [46,53,54]. Smaller ΔH/M values of ternary alloys containing Ti, Nb and Ni at 300–450 ºC temperature range compared to the $Pd_{65.1}Cu_{34.9}$ sample may be therefore attributed to their higher Cu concentrations. Nevertheless, none of the Ti, Nb and Ni elemental additions shows a significant effect for improving the hydrogen solubility. Furthermore, the effect of Ni in reducing the hydrogen solubility by stabilising α phase in Pd–Cu–Ni alloys was reported [35]. This effect is also reflected in our result as the ternary alloy containing Ni (Fig. 3d) exhibits the lowest hydrogen solubility compared to the ternary alloys containing Ti and Nb. In addition, although the ternary alloy containing V (Fig. 3e) has a lower Cu content compared to the $Pd_{65.1}Cu_{34.9}$ sample, it shows smaller ΔH/M values at temperatures higher than 300 ºC. Thus, it can be concluded that V addition also has a limiting effect on the hydrogen solubility.

Interestingly, additions of Y and Zr seem to significantly increase the hydrogen solubility in the ternary alloys (Fig. 3 f and g), despite their higher Cu concentrations compared to the $Pd_{65.1}Cu_{34.9}$ alloy. Whilst, the ΔH/M values for ternary alloys containing Y and Zr are about 2 times more than the $Pd_{65.1}Cu_{34.9}$ alloy at room temperature, their ΔH/M values show slightly less than 2 order increase in magnitude at 300 ºC (Fig.3f–g and Table S1). Furthermore, Pd–Cu–Y alloy shows a higher ΔH/M value at room temperature compared

to Pd–Cu–Zr alloy. However, a higher ΔH/M value can be seen for the Pd–Cu–Zr alloy at temperatures higher than 300 ºC compared to the Pd–Cu–Y alloy. Variation of hydrogen solubility in Pd–Cu–M (M: additive metal) alloys were also investigated by Density Functional Theory (DFT) calculations [32] and it was suggested that addition of M (M: Nb, Zr, Ti, and V) elements leads to a less favourable hydrogen binding in Octahedral sites (O sites) in fcc structure. Our results appears to confirm the DFT calculations in the case of hydrogen solubility reduction observed by adding V, Ni and the fact that no appreciable hydrogen solubility improvement was achieved by Ti and Nb additions. However, we may suggest Y and Zr additions result in a significant improvement in the hydrogen solubility.

Hydrogen diffusion coefficients of the Pd–Cu and Pd–Cu–M alloys are shown in Fig. 4 as a function of reciprocal temperature (Table S3 in supporting information for hydrogen diffusion coefficient data points). Hydrogen diffusion coefficient values for the $Pd_{65.1}Cu_{34.9}$ alloy vary from 1.9×10^{-5} to 5.7×10^{-5} over the 300 to 450 °C temperature range. These values are within the reported range for fcc Pd–Cu alloys [1,**Error! Reference source not found.**,55,57]. All ternary alloys show a lower diffusion coefficient compared to the $Pd_{65.1}Cu_{34.9}$ alloy within the studied temperature range except Ni, which shows a comparable diffusion coefficient to the $Pd_{65.1}Cu_{34.9}$ alloy at 450 °C. Whilst, ternary alloy containing Ni shows the least reduction in diffusion coefficient, ternary alloys containing Zr shows the greatest decreases in diffusion coefficient compared to the $Pd_{65.1}Cu_{34.9}$ alloy. The correlation between Cu concentration and hydrogen diffusivity in fcc Pd–Cu alloys were theoretically investigated [55,57] and it was shown that hydrogen diffusivity decreases with increasing Cu content. However, this effect is temperature dependent as the decrease in the hydrogen diffusivity becomes less significant with increasing temperature. Furthermore, room temperature hydrogen diffusivity in Pd–Cu alloys was suggested **Error! Reference source not found.** to be determined by structural transformations rather than Cu concentrations either in its bcc or fcc phase. Here, it seems that adding the

selected elements reduce the hydrogen diffusivity in the ternary alloys within the studied temperature range. This effect is similar to the previously observed effect of Ag addition for the reduced hydrogen diffusivity in Pd–Cu–Ag alloys [40]. This assumption is further supported by the lower hydrogen diffusion of Pd–Cu–V alloy, despite its lower Cu content compared to the $Pd_{65.1}Cu_{34.9}$ alloy. Also, a noticeable difference between the hydrogen diffusivities of the ternary alloys with a very similar Cu content (ternary alloys containing Ti, Nb, Y, and Zr) suggests different potentials of these elements to restrain the hydrogen diffusivity.

3.3 Hydrogen permeability

It is known that the rate of hydrogen dissociation and recombination on the surface of thick (>10 micron) Pd and Pd alloy membranes is considerably faster when compared to the rate of hydrogen diffusion through the bulk of these membrane [4]. Hence, hydrogen permeability can be determined by equation (3).

$$J = \emptyset \frac{P_1^n - P_2^n}{l} \quad (3)$$

Where J is the hydrogen flux (mol m^{-2} s^{-1}), Ø is hydrogen permeability (mol m^{-1} s^{-1} $Pa^{-0.5}$), P_1 and P_2 are hydrogen pressures (Pa) on the upstream and downstream sides of the membrane respectively, n is pressure exponent, which is 0.5 for bulk diffusion, and l is the membrane thickness (m).

Hydrogen permeability of the alloys studied here are compared with the literature reported hydrogen permeability of the corresponding Pd–Cu alloys at 350 °C [11,13] in Fig 5. Hydrogen permeability of our $Pd_{65.1}Cu_{34.9}$ alloy shows an excellent match with the reported literature value. Whilst ternary alloys containing Zr and Y show almost similar hydrogen permeability to their corresponding binary alloys, Pd–Cu–Ti alloy seems to have slightly lower hydrogen permeability in comparison to its binary alloy. Ternary alloys containing Ni, Nb, and V also show lower hydrogen permeabilities compared to their binary alloys. In addition, hydrogen permeability measurements of the ternary alloys between 300–500 °C are

shown in Fig. 6a–f (also Table S4 of supporting information). Ternary alloys containing Zr and Y show the highest hydrogen permeability within the studied temperature range respectively, despite their inferior hydrogen diffusivity values amongst the ternary alloys (Fig. 4). On the other hand, whilst Pd–Cu–Ni alloy showed the highest hydrogen diffusivity value (Fig. 4) compared to the other ternary alloys, its hydrogen permeability in Fig. 6c is lower than that of ternary alloys containing Zr and Y, which may be as a result of the marked effect of Ni in reducing the hydrogen solubility (Fig 3d). Thus, it seems that variations in the hydrogen permeabilities of the studied ternary alloys are mainly dominated by the variations of the hydrogen solubility rather than diffusivity. It was previously shown that whilst hydrogen solubility enhancement in the fcc Pd–Cu alloys could significantly improve the hydrogen permeation, variation in the hydrogen diffusivity had a less significant effect on the overall hydrogen permeation [40]. Similar effects are observed here (Fig. 5 and Fig.6) where ternary alloys containing Zr and Y, with the highest hydrogen solubilities amongst the ternary alloys studied, showed comparable hydrogen permeabilities to their corresponding binary alloys and higher hydrogen permeabilites than the other ternary alloys despite their lowest hydrogen diffusivity. Nevertheless, it has been noted that the contribution of bulk diffusion processes can be minimised by reducing the thickness of the membrane to less than 10 μm [4]. It has also been reported that [38] hydrogen permeability in thin film (~2 μm) $Pd_{73}Cu_{26}Y_1$ alloy could be increased by as much as 45% compared to corresponding Pd–Cu binary alloy. Thus, the significant enhancements in the hydrogen solubility achieved by Zr and Y suggest these elements are effective alloying elements to improve hydrogen permeability in the fcc phase of Pd–Cu alloys, providing that the contribution of the bulk diffusion could be minimised by a thickness reduction of the membrane.

3.4 Membrane poisoning by H_2S

Figure 7 shows the relative hydrogen flux of the studied membranes after switching pure hydrogen feed gas to H_2+1000 ppm H_2S gas mixture at 450 °C after completing hydrogen permeation measurements. Pd–Cu–Ni alloy shows inferior stability under H_2S containing atmosphere as the minimum hydrogen flux observed after 6 h is suppressed upon 8 h of H_2S exposure. Pd–Cu–V alloy shows only slightly better stability compared to Pd–Cu–Ni alloy with a slower rate of hydrogen flux reduction. Ternary alloys containing Ti, Y, and Nb show almost a similar stability compared to the $Pd_{65.1}Cu_{34.9}$ alloy. Interestingly, Pd–Cu–Zr alloy shows a noticeable stability improvement in comparison with the $Pd_{65.1}Cu_{34.9}$ alloy. Whilst the relative hydrogen flux through $Pd_{65.1}Cu_{34.9}$ and ternary alloys containing Ti, Y, and Nb is halved by falling to 50% of its original value after 8 h of H_2S exposure, the relative hydrogen flux in Pd–Cu–Zr alloy only falls to 65% of its original value. In addition, hydrogen flux is only reduced to less than 10% after 3 h of H_2S exposure in $Pd_{65.1}Cu_{34.9}$ and ternary alloys containing Ti, Y, Nb, and Zr, whereas ternary alloys containing Ni and V show instant hydrogen flux reductions. Reduction in the surface catalytic activity of Pd in Pd–based membranes, as a result of sulphur adsorption on the surface, is known [59,6] to be the responsible mechanism for initial decay in hydrogen flux after starting H_2S exposure. Nevertheless, hydrogen flux only ceases after the subsequent growth of surface sulphides and bulk sulfidation of the membrane. Hence, the minimal reduction in hydrogen flux observed in $Pd_{65.1}Cu_{34.9}$ and ternary alloys containing Ti, Y, Nb, and Zr up to 3 h of H_2S exposure may be related to the limited hydrogen dissociation on the membranes surface. Additionally, the formation and growth of less hydrogen permeable sulphides [59] is probably the dominant mechanism for higher rate of hydrogen reduction and its complete suppression at prolonged H_2S exposure. On the other hand, ternary alloys containing V and Ni seem more prone to S–surface interaction leading to the enhanced blocking of catalytic active sites for hydrogen

dissociation as well as formation and growth of sulphide phases. The dependency of sulfidation process in Pd–Cu alloys to the H_2S:H_2 ratio and the operation temperature has been previously shown [23,25]. The high concentration of H_2S in our feed gas satisfies the thermodynamic requirement[25] for sulfidation in all the studied Pd–Cu alloys. XRD patterns in Fig. 8a–g show the structure of the alloys after H_2S exposure. All samples show the formation of Pd_4S/Cu_2S sulphides after H_2S exposure. Whilst formation of Pd_4S phase as a dominant phase is thermodynamically predicted[25] at the current experimental condition, Fig. 8a–g shows that Pd_4S is not the main sulphide phase. Studies[23,25] show a high affinity of Cu to sulphur may lead to Cu segregation in H_2S exposed Pd–Cu alloys, drifting the alloy composition from ideal solid solution. Similarly, Cu_2S seems to be the dominant sulphide phase in all our H_2S exposed alloys. Cu segregation toward the surface of the alloys also leads to the formation Cu rich Cu–Pd (Cu–Ti in Pd–Cu–Ti alloy) phases. Nevertheless, Pd–Cu–Zr alloy seems to be more resistant to the Cu segregation and therefore sulfidation as a result of its structural stability. Interestingly, Fig. 8g shows Pd–Cu–Zr alloy preserves its texture along (220) plane after H_2S exposure, further reflecting the structural stability of this alloy. The structural stability of this alloy can significantly slow down the Cu segregation throughout H_2S exposure which seems to have a primary role on alloys sulfidation. Overall, a small amount of Zr in Pd–Cu–Zr alloy may effectively induce structural stability as reflected by stable (220) texture and sluggish sulfidation kinetic.

4 Discussion

The effects of elemental Ag addition on the hydrogen diffusivity and solubility of fcc and bcc Pd–Cu alloys were extensively investigated in our previous report [40] using theoretical studies considering hydrogen diffusivity and solubility mechanisms in bcc and fcc alloys [32-34,48]. Unlike the identical effects of additional elements used in this study for decreasing hydrogen diffusivity, their effects on hydrogen solubility seem to be more complex.

It is known that hydrogen atoms can occupy either Octahedral (O site), or Tetrahedral (T site) site in the disordered fcc Pd–Cu alloys. At high temperatures, hydrogen diffuses by hopping through various O and T sites after overcoming a Transition State (TS) energy barrier[33,48]. The disordered nature of the fcc phase implies the existence of various energetically distinct sites with varying diffusion activation energies. Thus, hydrogen diffusion is controlled by both binding energies and the transitions state energies for individual hops [34,48]. DFT calculations show [34] that replacing a small amount of Ag for Cu in Pd–Cu fcc phase results in more favourable hydrogen bonding in interstitial sites. In addition, TS energy for an alloy is not constant but, rather determines by the alloy's composition at near atomic neighbour level [58]. This was theoretically shown [34] to be true in Pd–Cu–Ag alloys by observation of a higher activation energy barrier for hydrogen hopping through TS having one or more Ag atoms. Furthermore, TS energy can be influenced by lattice size variation as a consequence of alloying [51]. Whilst expanded lattice is suggested to reduce the activation energy, *i.e.* an increase in the rate of hydrogen hopping, the reverse is true for lattice contraction. However, despite the observed lattice expansions for the Pd–Cu–Ag alloys lower hydrogen diffusivity values were constantly observed at high temperatures compared to binary alloys [40], which may indicate a minimal effect of lattice expansion on the overall hydrogen diffusivity in such a ternary alloy. Also, it was suggested [51] that alloying with additional elements having a larger atomic size compared to the alloys constituent elements can increase T site energy and therefore encouraging direct hydrogen hopping between two O sites. Therefore, reductions in hydrogen diffusivities observed in Fig. 4 may be attributed to the influence of alloying elements on ease of hydrogen hopping and its preferred route by affecting O sites, T sites and TS energies as a result of altering local atomic compositions.

The dependence of hydrogen solubility on lattice size in Pd–alloys have been reported [33,38]. For example, isoelectronic Pd–Y_8 and Pd–Ag_{24} alloys show higher hydrogen solubility

than pure Pd where their lattice size is 29% and 5% larger than pure Pd respectively [42]. In addition, similar improvement in hydrogen solubility was theoretically predicted due to the lattice expansion in Pd–Cu–Ag alloys [34]. However, it is known that changes in hydrogen solubility cannot be described solely based on the variation in lattice size [34,40]. Subsequently, other factors such as the accessibility of free atomic sites for hydrogen occupancy [34,60], chemical potential of alloys–hydrogen system [44] and the effect of solute valence electrons [49,50,61] were envisaged to play an important role for hydrogen solubility. For example, it was suggested that [60] increasing alloying atoms in the nearest neighbours (NN) favours hydrogen absorption only up to a certain extent that is 50% of total capacity of NN. This was further confirmed [34] in Pd–Cu–Ag alloys where an increase in Ag content led to less favourable binding energies of hydrogen in O sites. The existence of more Ag in NN shell of the interstitial site in Pd–Cu–Ag alloy could limit the accessibility of the free inferential space for hydrogen occupation. Furthermore a stronger interaction between alloys and hydrogen is known to encourage hydrogen solubility in Pd alloys [44]. This can be translates into the chemical potential of alloy–hydrogen system depending on ionic diameter and interaction free energy of hydrogen–solute metal pair. Finally, the electronic effect of additional elements on the hydrogen solubility was assumed to be mainly dominated by solute valence electrons as hydrogen solubility decreased once more Pd 4d-bands were occupied in spite of additional lattice expansion [49,50,61]. Additionally, small changes in alloys charge density which is a function of atomic size of alloying elements and their and electronegativity, may have an impact on the stability of hydrogen in different interstitial sites [62].

In this study, low concentrations of additional elements were chosen with the purpose of minimising their limiting effects on the accessibility of free interstitial sites for hydrogen occupation. Atomic radius, effective valence, and enthalpy of hydride formation for additional elements in this study (Y, Ti, Zr, V, Nb, and Ni) are listed in Table 1. If the

observed hydrogen solubility values for Pd–Cu–Zr sample at temperatures higher than 100 °C is excluded (which will be discussed later), the Pd–Cu–Y alloy shows the highest hydrogen solubility values. It can be seen in Table 1 that yttrium best matches the requirements for improved hydrogen solubility, having the largest atomic radius, the lowest valence electron and highest affinity to hydrogen compared to other additional elements. Similarly, Ni shows significant reduction in hydrogen solubility because of its minimal effect for lattice expansion, higher valance electron compared to Cu and least interaction with hydrogen. In general, it seems that the effects of these elements (except Zr) can be relatively described by their ability to fulfil the mentioned requirements for improving hydrogen solubility.

Lower hydrogen solubility values at temperatures below 100 °C can be observed for Pd–Cu–Zr sample when compared to the ternary alloy containing Y with almost identical Pd and Cu contents. This may be expected from smaller lattice expansion achieved by Zr addition, its higher effective valence and less interaction with hydrogen compared to Y. However, once the temperature is increased above 100 °C, Pd–Cu–Zr sample shows higher hydrogen solubility values. Higher hydrogen solubility values of Pd–Cu–Zr versus Pd–Cu–Y sample at higher temperatures may be explained by the contribution of other factors influencing the overall hydrogen solubility. For instance, it is known that [63,64] an increase in the defect density within the microstructure can substantially enhance hydrogen solubility due to the trapping effect. Dislocations, point defects, and precipitate-matrix areas, which are introduced into the microstructure by various techniques such as plastic deformation and heat treatment, can significantly increase hydrogen solubility, although these features are detrimental to diffusivity. Dilute additions of Zr in a pure aluminium matrix have been shown [65] to improve the thermal stability and retention of small grains of the sample up to temperatures higher than 300 °C. Also, solution hardening and consequent thermal cyclic

stability was reported in Cu–Zr alloys [66]. Minute solubility of Zr in Cu led to precipitation, which could effectively stabilise the microstructure. Similarly, structural stabilisation was observed in our Pd–Cu–Zr sample after heat treating under vacuum (Fig. 1n) and under H_2S containing atmosphere (Fig. 8g). In addition, we have investigated the structural stability of Pd–Cu–Zr sample under hydrogen atmosphere at various temperatures in Fig. 9. It can be seen that Pd–Cu–Zr sample retains its (220) texture up to temperatures as high as 600 °C, which implies to microstructural stability of the sample. Hence, the greater stability of hydrogen solution at higher temperatures in the Pd–Cu–Zr sample could be due to the trapping of a proportion of the hydrogen atoms by lattice defects induced by cold rolling.

Chemical composition (surface reactivity) and electronic structure of Pd–based membranes can be altered by alloying [7,31,67]. Hence, alloying can have a notable effect on the performance of the membrane under impurity gases. For instance, whilst Pd has a stronger interaction with S compared to Cu, weaker S absorption energies are in general observed on the Pd–Cu alloys surfaces [5]. Alloying effect in Pd–Cu alloys was also studied by Ling *et al.* [68] and binding sites were shown to be spatially heterogeneous in $Pd_{75}Cu_{25}$ alloy when compared to pure Pd. Although these binding sites share a similar geometry, the atomic composition varies locally. In addition, electronic structure of Pd and Pd alloys may have a substantial effect on the S–surface interaction [5,7,31]. Pd–Cu–Zr alloy with the preserved (220) texture may possess a different surface atomic composition as a result of Zr addition. Thus, S–surface interaction may become less favourable in this alloy as Zr addition can potentially create new binding sites on the surface with distinctive binding energies. Moreover, the structural stability of Pd–Cu–Zr alloy may also improve resistance to sulphur poisoning by reducing the elemental segregation under H_2S containing atmosphere. We may suggest that limited atomic diffusivity of Pd and especially Cu in Pd–Cu–Zr alloy can significantly retard the surface and bulk sulfidation kinetic in this alloy.

In general, it seems that the structural stabilisation induced by adding a third element is a useful strategy for designing novel Pd–Cu–M (M: additional element) membranes with improved H_2S resistance. However, elemental alloying additions should also satisfy the requirements for improved hydrogen permeation through the membrane. We recently reported the improved resistance of Pd–Cu–Zr alloy to the sulphur poisoning[69]. The present work suggests the effects of Zr addition on the structure, surface properties and thermal stability of both bcc and fcc Pd–Cu alloys need to be further investigated and optimised.

5. Conclusions

Pd–Cu–M (M= Y, Ti, Zr, V, Nb, and Ni) alloys with a small amount (1–2.6 at.%) of M elements were investigated as potential hydrogen purification membranes. Structural analyses by XRD suggested Zr addition improves structural stability in Pd–Cu–Zr alloy, leading to the preserved surface texture (induced by cold rolling) after heat treatment at 650 °C for 96 h. The greatest lattice expansion was observed with Y addition, which could be explained by its bigger atomic size compared to Cu. However, variations in the lattice parameters upon addition of Ni and V with a similar atomic size to Cu suggested possible contributions from the solute valence electrons to the lattice size. Hydrogen solubilities of the ternary alloys were measured and significant increase in the hydrogen solubility values were noted for the ternary alloys containing Y and Zr. Whilst, V and Ni seemed to reduce the hydrogen solubility, no significant effect on the hydrogen solubility was observed by Ti and Nb additions. The effects of small additions of third elements on the hydrogen solubility seemed to be related to a combination of their atomic size, valence electron and their affinity to hydrogen, except for the Pd–Cu–Zr sample. Higher hydrogen solubility observed at temperatures above 100 °C for Pd–Cu–Zr sample, when compared to Pd–Cu–Y, was attributed to the hydrogen trapping by relatively stable defective sites as a result of structural stability induced by Zr addition. Furthermore, additions of all the alloying elements decreased

the hydrogen diffusivity by increasing the required energy for hydrogen hopping within the bulk of the samples with Zr having the greatest and Ni showing the least effect. The comparable hydrogen permeabilities of ternary alloys containing Zr and Y to the respecting binary alloys despite their reduced hydrogen diffusivity, further confirmed that hydrogen permeability in fcc phase of Pd–Cu alloys is mainly dominated by hydrogen solubility. A superior resistance to sulphur poisoning was observed for the Pd–Cu–Zr alloy when exposed to 1000 ppm H_2S+H_2 gas mixture. This was attributed to the preserved texture and changes to the alloy electronic structure as a result of a small Zr addition. Nevertheless, we may propose that the structural stability of Pd–Cu–Zr alloy plays a key role for improving the alloy resistance to sulphur poisoning by limiting the atomic diffusion and segregation of Pd and Cu elements, slowing surface and bulk sulfidation kinetic.

Supporting Information

Cross sectional EDS analyses of annealed alloy, hydrogen solubility values of $Pd_{65.1}Cu_{34.9}$ and ternary Pd–Cu–M alloys, hydrogen diffusivity values of $Pd_{65.1}Cu_{34.9}$ and ternary Pd–Cu–M alloys, hydrogen permeability values of $Pd_{65.1}Cu_{34.9}$ and ternary Pd–Cu–M alloys

Acknowledgments

Supports from the EPSRC SUPERGEN Delivery of Sustainable Hydrogen (EP/G01244X/1), the Birmingham Science City Hydrogen Energy projects and the Hydrogen and Fuel Cell Research Hub are gratefully acknowledged.

Refrences:

1. Alefeld, G.; Völkl, J.; (Eds.) Hydrogen in Metals I and II, Springer-Verlag, Berlin, 1978.
2. Dittmeyer, R.; Höllein, V.; Duab, K. Membrane Reactors for Hydrogenation and Dehydrogenation Processes Based on Supported Palladium J. Mol. Catal. A: Chem. 2001, 173, 135-184
3. Knapton, A.G. Palladium Alloys for Hydrogen Diffusion Membranes Platinum Met. Rev. 1977, 21, 2, , 44-50

4. Yun, S.; Oyama, S. T.; Correlation in Palladium Membranes for Hydrogen Seperation: A review J. Membr. Sci. 2011, 375, 28-45
5. Alfonso, D. R.; Cugini, A. V.; Sholl, D. S. Density Functional Theory Studies of Sulphur Binding on Pd, Cu and Ag and Their Alloys Surf. Sci. 2003, 546, 12-26
6. Gabitto, J. F.; Tsouris, C. Sulphur Poisoning of Metal Membranes for Hydrogen Separation IRECHE 2009,1, 5, 394-411
7. Ozdogan, E.; Wilcox, J. Investigation of H_2 and H_2S Adsorption on Niobium- and Copper Doped Palladium Surfaces J. Phys. Chem. B 2010, 114, 12851-12858
8. Paglieri, S.N.; Way, J.D. Innovation in Palladium Membrane Research Sep. Purif. Methods 2002, 31, 1, 1-169
9. Basile, A.; Gallucci, F.; Tosti, S. Synthesis, Characterisation, and Application of Palladium Membranes Membr. Sci. Technol. 2008, 13, 255-323
10. Gallucci, F.; Fernandez, E.; Corengia, P.; Annaland, M. V. S. Recent Advances on Membrane Reactors for Hydrogen Production Chem. Eng. Sci. 2013, 92, 40-66
11. . McKinley, D. L. Methods for Hydrogen Separation and Purification US patent 1969, 3,439,474
12. Roa, F.; Block, M. J.; Way, J. D. The Influence of Alloy Composition on the H_2 flux of Composite Pd-Cu Membranes Desalination 2002,147 , 411-416
13. Howard, B. H.; Killmeyer, R. P.; Rothenberger, K. S; Cugini, A.V.; Morreale, B. D.; Enick, R. M.; Bustamante, F. Hydrogen Permeance of Palladium-Copper Alloy Membranes Over a Wide Range of Temperatures and Pressures J. Membr. Sci. 2004, 241, 207-218
14. Yuan, L.; Goldbach, A.; Xu, H. Segregation and H_2 Transport Rate Control in Body-Centered Cubic PdCu Membranes J. Phys. Chem. B 2007, 111, 10952-10958
15. Opalka, S. M.; Huang, W.; Wang, D.; Flanagan, T.B.; LØvvik, O.M.; Emerson, S.C.; She, Y.; Vanderspurt, T. H. Hydrogen Interaction with the PdCu Ordered B2 alloy J. Alloys Compd. 2007, 44-447, 583-587
16. Yuan, L.; Goldbach, A.; Xu, H. Real-Time Monitoring of Metal Deposition and Segregation Phenomena During Preparation of PdCu Membranes J. Membr. Sci. 2008, 322, 39-45
17. Yuan, L.; Goldbach, A.; Xu, H. Permeation Hysteresis in PdCu Membranes J. Phys. Chem. B 2008,112, 12692-12695
18. Goldbach, A.; Yuan, L.; Xu, H. Impact of the fcc/bcc Phase Transition on the Homogeneity and Behavior of PdCu Membranes Sep. Purif. Technol. 2010,73, 65-70
19. Morreale, B. D.; Ciocco, M. V.; Howard, B. H.; Killmeyer, R. P.; Cugini, A.V.; Enick, R. M. Effect of Hydrogen-Sulfide on the Hydrogen Permeance of Palladium-Copper Alloys at Elevated Temperatures J. Membr. Sci. 2004, 241, 219-224
20. Subramanian, P.R.; Laughlin, D.E. Cu-Pd (Copper-Palladium) J. Phase Equilib.1991, 12, 2, 231-243piper
21. Kamakoti, P.; Morreale, B. D.; Ciocco, M.V.; Howard, B.H.; Killmeyer, R.T. Cugini, A.V.; Sholl, D.S. Prediction of Hydrogen Flux Through Sulphur-Tolerant Binary Alloy Membrane Science 2005, 307, 569-573
22. O'Brien, C P.; Howard, B. H.; Miller, J. B.; Morreale, B. D. Gellman, A. J. Inhibition of Hydrogen Transport Through Pd and $Pd_{47}Cu_{53}$ Membranes by H_2S at 350 ºC J. Membr. Sci. 2010, 349, 380-384
23. Kulprathipanja, A.; Alptekin, G.O.; Falconer, J.L.; Way, J.D. Pd and Pd-Cu Membrane: Inhibition of H_2 Permeation by H_2S J. Membr. Sci. 2005, 254, 49-62
24. Peters, T.A.; Kaleta, T.; Stange, M. Bredesen, R. Hydrogen Transport through a Selection of Thin Pd-Alloy Membranes: Membrane Stability, H_2S Inhibition, and

Flux Recovery in Hydrogen and Simulated WGS Mixtures Catal. Today 2012, 193, 8-19

25. Iyoha, O.; Enick, R.; Killmeyer, R.; Morreale, B. The Influence of Hydrogen Sulphide to Hydrogen Partial Pressure Ratio on the Sulfidization of Pd and 70 mol% Pd-Cu Membranes J. Membr. Sci. 2007, 305, 77-92
26. Opalka, S. M.: LØvvik, O. M.; Emerson, S. C. ; She, Y.; Vanderspurt, T. H. Electronic Origins for Sulphur Interactions with Palladium Alloys for Hydrogen-Selective Membranes J. Membr. Sci. 2011, 375, 96-103
27. Gade, S. K.; DeVoss, S. J.; Coulter, K. E.; Paglieri, S. N.; Alptekin, G. O.; Way, J. D. Palladium-Gold Membranes in Mixed Gas Streams with Hydrogen Sulphide: Effect of Alloy Content and Fabrication Technique J. Membr. Sci. 2010, 378, 35-41
28. Chen, C. H.; Ma, Y. H. The Effects of H_2S on the Performance of the Pd and Pd/Au Composite Membrane J. Membr. Sci. 2010, 362, 535-544
29. Braun, F.; Miller, J. B.; Gellman, A. J.; Traditi, A. M.; Fleutot, B.; Kondratyuk, P.; Cornaglia, L.M. PdAgAu Alloy with High Resistance to Corrosion by H_2S Int. J. Hydrogen Energy2012, 37, 18547-18555
30. Venezia, A. M.; La Parola, V.; Nicoli, V.; Deganello, G. Effect of Gold on the HDS Activity of Supported Palladium Catalysts J. Catal. 2002, 212, 56-62
31. Hyman, M. P.; Loveless, B. T.; Medlin, J. W. A Density Functional Theory Study of H_2S Decomposition on the (111) Surfaces of Model Pd-Alloys Surf. Sci.2007, 601, 5382-5393
32. Kamakoti, P.; Sholl, D.S. Towards First Principles-Based Identification of Ternary Alloys for Hydrogen Purification Methods J. Membr. Sci. 2006, 279, 94-99
33. Semidey-Flecha, L.; Ling, C.; Sholl, D.S. Detailed First Principles Models of Hydrogen Permeation Through PdCu-Based Ternary Alloys J. Membr. Sci. 2010, 362, 384-392
34. Ling, C.; Semidey-Flecha, L.; Sholl, D. S. First Principles Screening of PdCuAg Ternary Alloys as H_2 Purification Membranes J. Membr. Sci. 2011, 371, 189-196
35. Ryi, S. K.; Park, J. S.; Kim, S. H.; Kim, D. W.; Moon, J. W. Long Term Hydrogen Permeation Tests of Pd-Cu-Ni/PNS with Temperature Cycles from Room Temperature to 773K J. Membr. Sci. 2007, 306, 261-266
36. Tarditi, A. M.; Braun, F.; Cornaglia, L. M. Novel PdAgCu Ternary Alloys: Hydrogen Permeation and Surface Properties. Appl. Surf. Sci. 2011, 257, 6626
37. Tarditi, A. M.; Cornaglia, L. M. Novel PdAgCu Ternary Alloys as Promising Materials for Hydrogen Separation Membranes: Synthesis and Characterisation Surf. Sci. 2011, 605, 62-71
38. Peters, T. A.; Kaleta, T.; Stange, M.; Bredesen, R. Development of Thin Binary and Ternary Pd-Based Alloys Membranes for Use in Hydrogen Production J. Membr. Sci. 2011, 383, 124-134
39. Dogan, Ö. N.; Hu, R.; Song, X.; Chen, S.; Gao, M. C. Ordered Bcc Phases in a Cu-Pd-Mg Hydrogen Separation Membrane Alloy J. Alloys Compd. 2012, 528, 10-15
40. Nayebossadri, S.; Speight, J.; Book, D. Effects of Low Ag Additions on the Hydrogen Permeability of Pd–Cu–Ag Hydrogen Separation Membranes J. Membr. Sci. 2014, 451, 216-225
41. Fletcher, S. Thin-Film Palladium-Yttrium Membranes for Hydrogen Separation. PhD thesis, University of Birmingham, 2009
42. Hughes, D. T.; Harris, I. R. A Comparative Study of Hydrogen Permeabilities and Solubilities in Some Palladium Solid Solution Alloys J. Less-Common Met. 1978, 61, P9-P21
43. Slater, J. C. Atomic Radii in Crystals J. Chem. Phys. 1964, 41, 3199-3204

44. Ramaprabhu, S. Thermodynamics and Stability of Dissolved Hydrogenation in Pd Rich Binary $Pd_{1-x}Z_x$ and Ternary $Pd_{1-x}Z_xZ'_y$ Solid Solution Alloys Int. J. Hydrogen Energy 1998, 23, 9, 787-795
45. Wang, Y.B.; Northwood, D. O. Calculation of the Enthalpy of Metal Hydride Formation J. Less-Common Met. 1987, 135, 239-245
46. Burch, R.; Buss, R.G. Absorption of Hydrogen by Palladium-Copper Alloys J. Chem. Soc., Faraday Trans. 1975, 1, 71, 913-921
47. Fisher, D., Chisdes, D.M.; Flanagan, T. B. Solution of Hydrogen in Palladium/Copper Alloys. J. Solid State Chem. 1977, 20, 149-158
48. Kamakoti, P.; Sholl, D.S.; A Comparison of Hydrogen Diffusivities in Pd and CuPd Alloys Using Density Functional Theory J. Membr. Sci. 2003, 225, 145-154
49. Harris, I. R.; Norman, M. Observation on the Lattice Spacing of some α Pd-X Solid Solutions and some Pd_3X Phases J. Less-Common Met.1970, 22, 127-130
50. Doyle, M. L.; Harris, I. R. Palladium–Rare Earth Alloys: Their Order-Disorder Transformations and Behaviour with Hydrogen Platinum Met. Rev.1988, 32, 3, 130-140
51. Semidey-Flecha, L.; Sholl, D. S. Combining Density Functional Theory and Cluster Expansion Methods to Predict H_2 Permeance Through Pd-Based Binary Alloy Membranes J. Chem. Phys. 2008, 128, 144701-144710
52. Martin, M. H.; Galipaud, J.; Tranchot, A.; Roué, L.; Guay, D. Measurements of Hydrogen Solubility in CxPd100-x Thin Films, Electrochim Acta2013, 90, 615-622
53. Burch, R.; Buss, R. G. Pressure Composition Isotherms in the Palladium–Copper–Hydrogen System Solid State Commun. 1974, 15, 407-409
54. Flanagan T. B.; Chisdes, D. M. Solubility of Hydrogen (1 atm, 298 K) in some Copper/Palladium Alloys Solid State Commun. 1975, 16, 529-532
55. Kamakoti, P.; Sholl, S. Ab Initio Lattice-Gas Modelling of Interstitial Hydrogen Diffusion in CuPd Alloys Phys. Rev.B 2005, 71, 14301-14309
56. Piper, J. Diffusion of Hydrogen in Copper-Palladium Alloys J. Appl. Phys. 1966, 37, 2, 715-721
57. Qin, L.; Jiang, C. First–Principles Based Modelling of Hydrogen Permeation Through Pd–Cu alloys Int. J. Hydrogen Energy2012, 37, 17, 12760-12764
58. Sonwane, C. G.; Wilcox, J.; Ma, Y. H. Achieving Optimum Hydrogen Permeability in PdAg and PdAu alloy J. Chem. Phys. 2006, 125, 184714-184724
59. Morreale, B.D.; Howard, B.H.; Iyoha, O.; Enick, R.M.; Ling, C.; Sholl, D.S. Experimental and Computational Prediction of the Hydrogen Transport Properties of Pd_4S Ind. Eng. Chem. Res. 2007,46, 19, 6313-6319
60. Sonwane, C.G.; Wilcox, J.; Ma, Y. H.; Solubility of Hydrogen in PdAg and PdAu Binary Alloys Using Density Functional Theory J. Phys. Chem. B 2006,110, 24549-24558
61. Fort, D.; Farr, J. P. G.; Harris, I. R. A Comparison of Palladium–Silver and Palladium–Yttrium Alloys as Hydrogen Separation Membranes J. Less-Common Met. 1975, 39, 293-308
62. Aboud, S.; Wilcox, J. A Density Functional Study of the Charge State of Hydrogen in Metal Hydrides J. Phys. Chem. C 2010, 114, 10978-10985
63. Dos Santos, D. S.; De Miranda, P. E. V. Hydrogen Solubility in Amorphous and Crystalline Materials Int. J. Hydrogen Energy1998, 23,11, 1011-1017
64. Smith, D. A.; Jones, I. P.; Harris, I. R. Lattice Order and Hydrogen Solublity in Pd_7Ce J. Less-Common Met. 1984, 103, 33-43

65. Hasegawa, H.; Komura, S.; Utsunomiya, A.; Horita, Z.; Furukawa, M.; Nemoto, M.; Langdon, T. G. Thermal Stability of Ultrafine-Grained Aluminium in the Presence of Mg and Zr Additions Mater. Sci. Eng., A 1999, 265, 188-196
66. Canadinc, D.; Niendorf, T.; Maier, H. J. A Comprehensive Evaluation of Parameters Governing the Cyclic Stability of Ultrafine-Grained fcc Alloy Mater. Sci. Eng., A 2011, 528, 6345-6355
67. Gao, H.; Lin, Y. S.; Li, Y.; Zhang, B. Chemical Stability and its Improvement of Palladium-Based Metallic Membranes Ind. Eng. Chem. Res. 2004, 43, 6920-6930
68. Ling, C.; Sholl, D. S. Using First Principles Calculations to Predict Surface Resistances to H_2 Transport through Metal Alloy Membrane J. Membr. Sci. 2007, 303, 162-172
69. Nayebossadri, S.; Speight, J. D; Book, D. A Novel Pd–Cu–Zr Hydrogen Separation Membrane with a High Tolerance to Sulphur Poisoning. Chem. Commun. 2015, 51, 15842-15845

Figures:

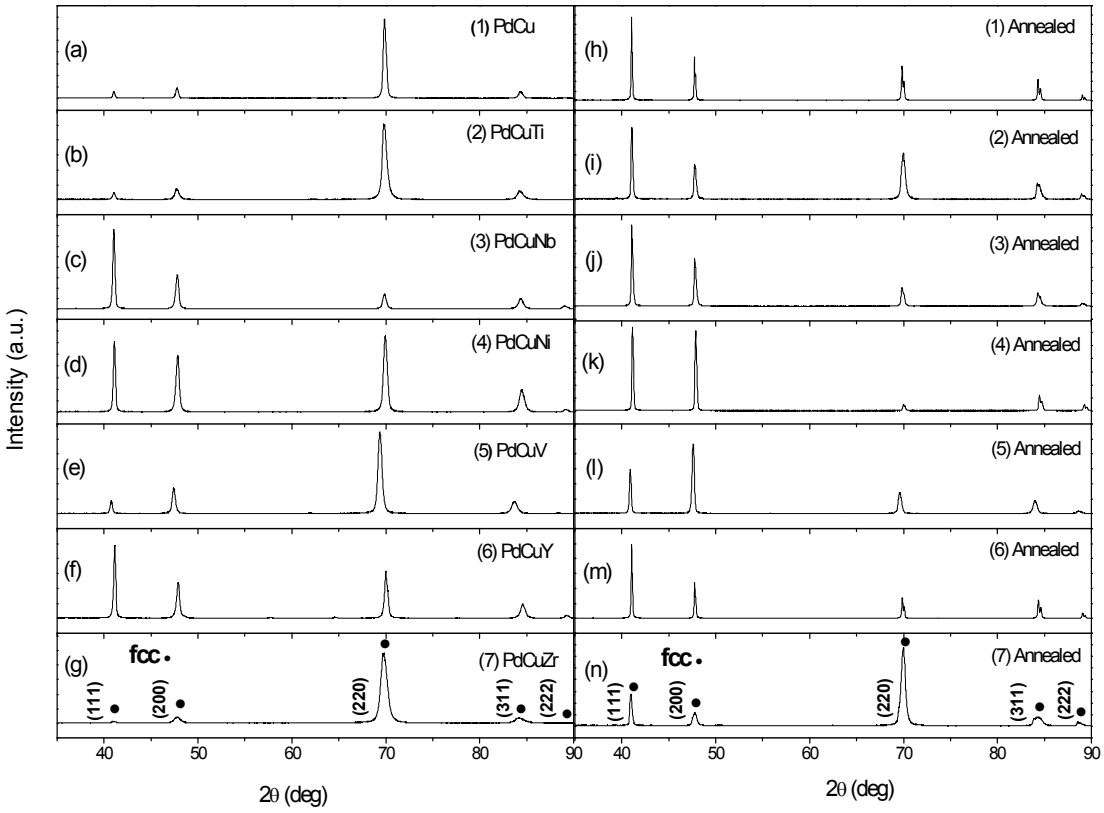

Figure 1: XRD patterns of as fabricated (a) $Pd_{65.1}Cu_{34.9}$ and Pd–Cu–M alloys with (b) Ti, (c) Nb, (d) Ni, (e) V, (f) Y, and (g) Zr. XRD diffraction patterns of annealled (h) $Pd_{65.1}Cu_{34.9}$ and Pd–Cu–M alloys with (i) Ti, (j) Nb, (k) Ni, (l) V, (m) Y, and (n) Zr at 650 °C for 96 h under vacuum.

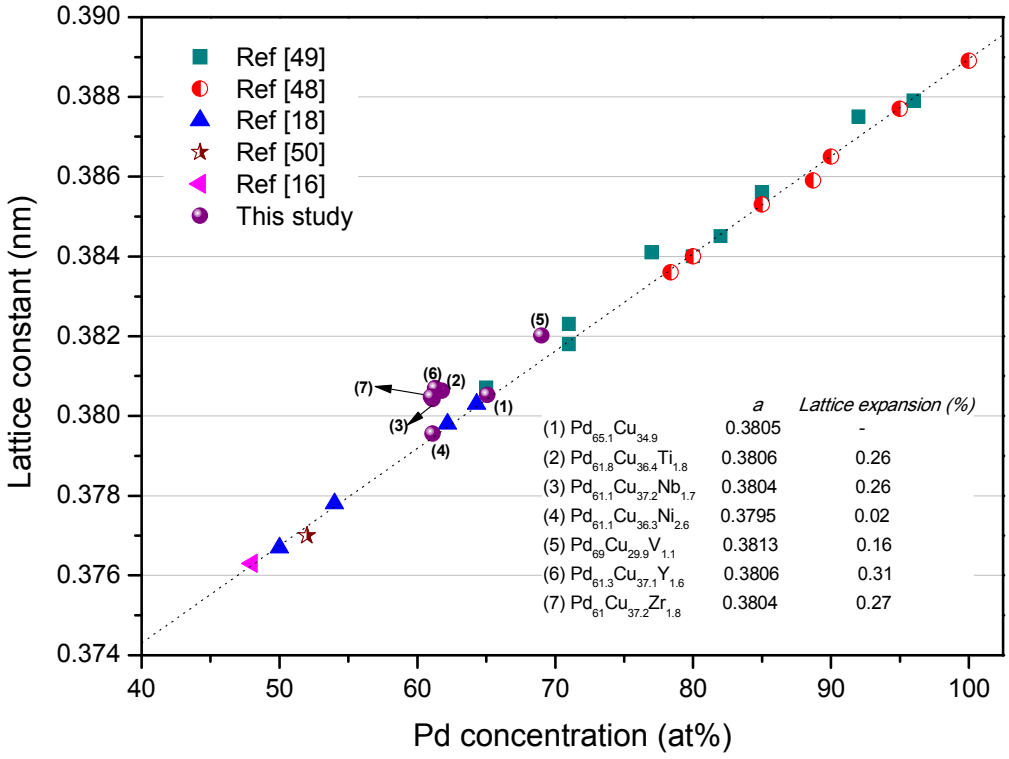

Figure 2: Lattice parameters of the fcc Pd–Cu alloys as a function of Pd concentration. Lattice parameters for the $Pd_{65.1}Cu_{34.9}$ and Pd–Cu–M (M= Y, Ti, Zr, V, Nb, and Ni) alloys are included for comparison. Also, lattice expansions values are listed inset. Dotted line is a guide to the eye.

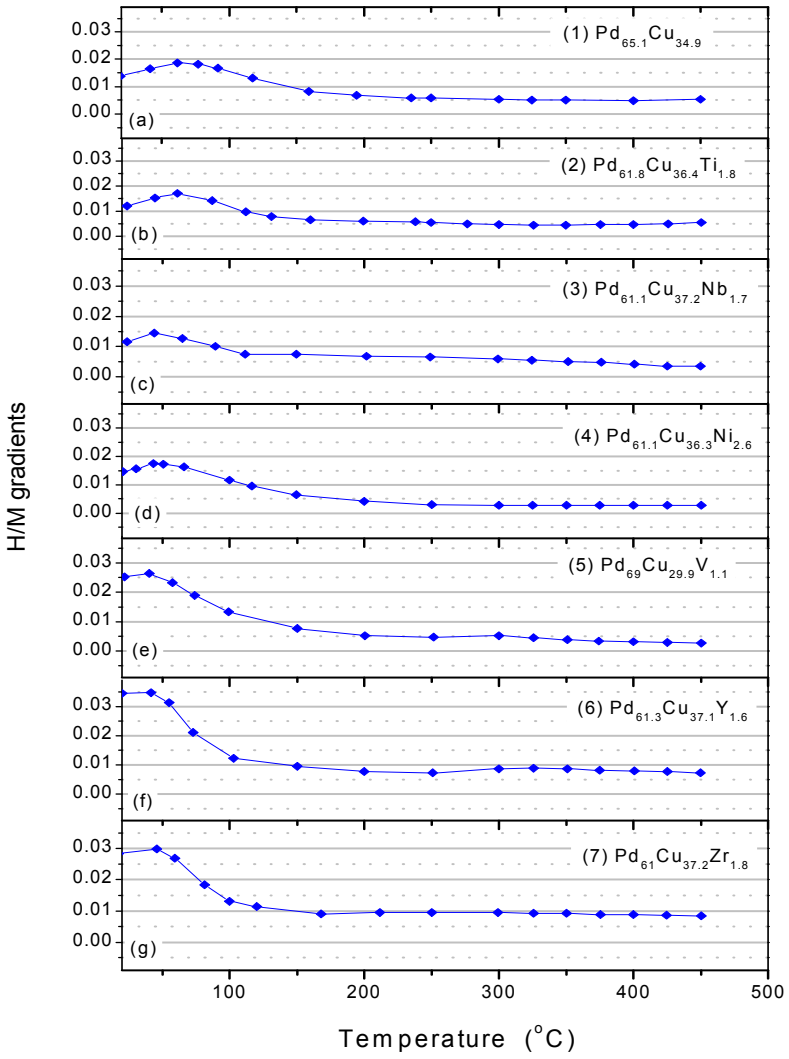

Figure 3: H/M gradients through the thickness of (a) $Pd_{65.1}Cu_{34.9}$ and Pd–Cu–M alloys with (b) Ti, (c) Nb, (d) Ni, (e) V, (f) Y, and (g) Zr from room temperature to 450 °C. H/M gradients were determined by subtracting H/M atomic ratios measured at 6.18 and 1 bar. A heating rate of 1 °C min^{-1} was applied. Data points are connected by guide lines.

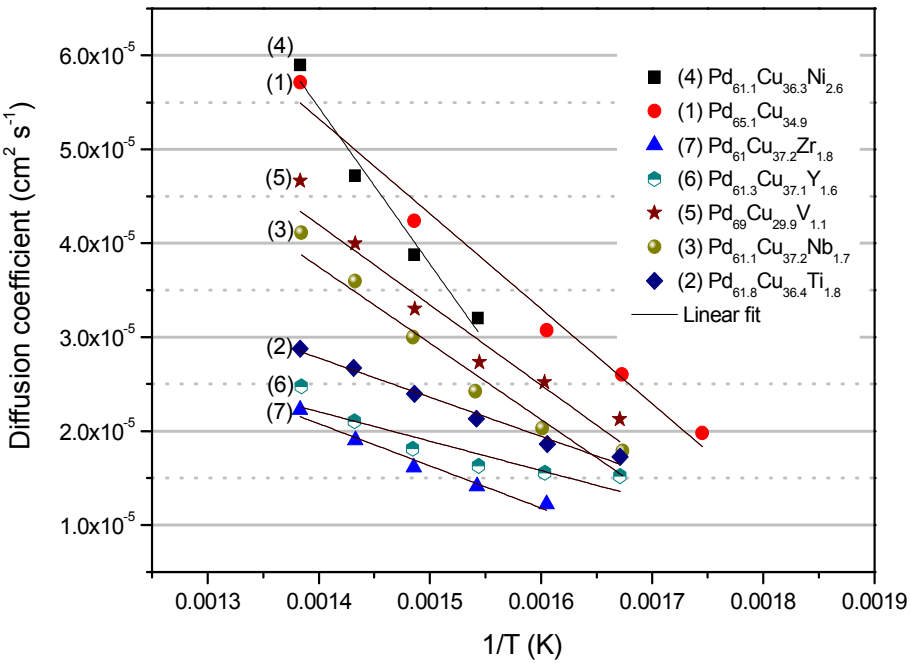

Figure 4: Hydrogen diffusion coefficients *D* as a function of inverse temperature for the $Pd_{65.1}Cu_{34.9}$ and Pd–Cu–M (M= Y, Ti, Zr, V, Nb, and Ni) alloys. Data points are connected by guide lines.

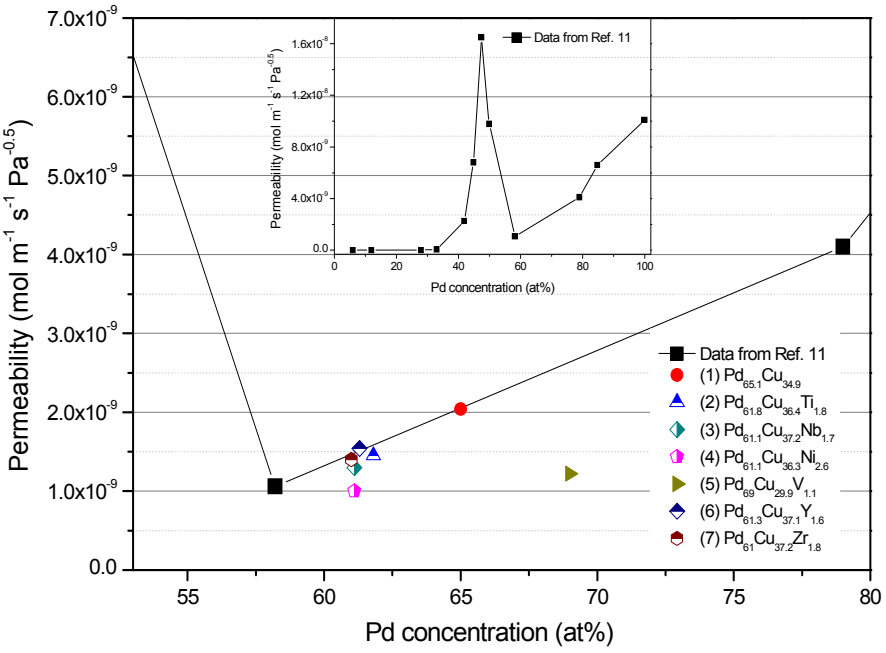

Figure 5:Comparing hydrogen permeability values of $Pd_{65.1}Cu_{34.9}$ and Pd–Cu–M (M= Y, Ti, Zr, V, Nb, and Ni) alloys to thier respecting binary alloys at 350 °C. The inset graph is hydrogen permeability values of the Pd–Cu alloys as a function of Pd consentration at 350 °C. Solid line is guide for the eye.

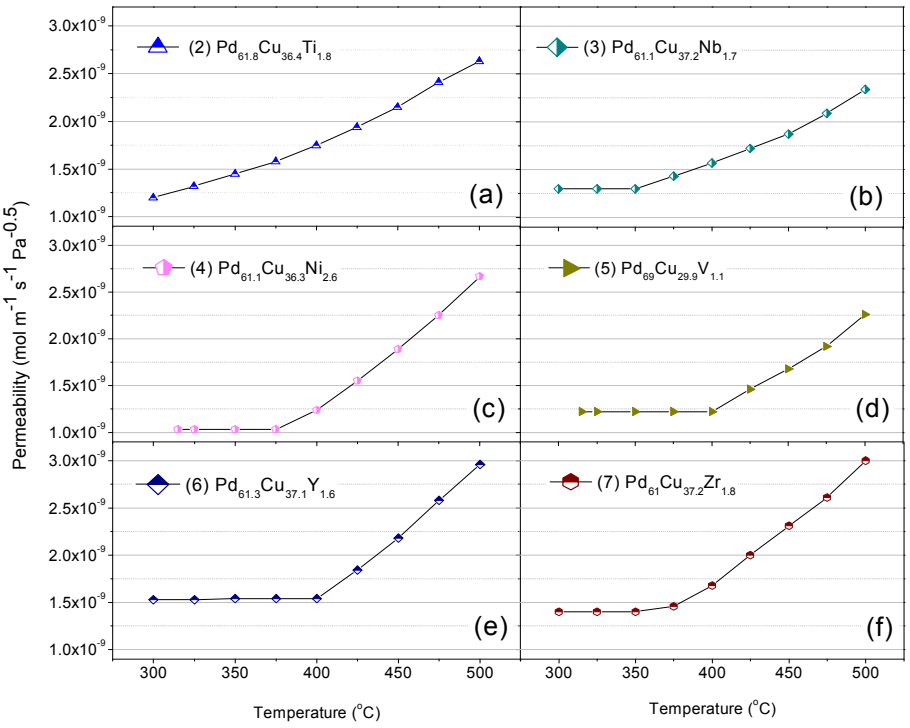

Figure 6: Hydrogen permeability profiles of Pd–Cu–M alloys with (a) Ti, (b) Nb, (c) Ni, (d) V, (e) Y, and (f) Zr additional elements as a function of temperature. A heating rate of 2°C min^{-1} was applied with a constant hydrogen pressures of 6.18 and 1 bar on the feed and permeate sides respectively.

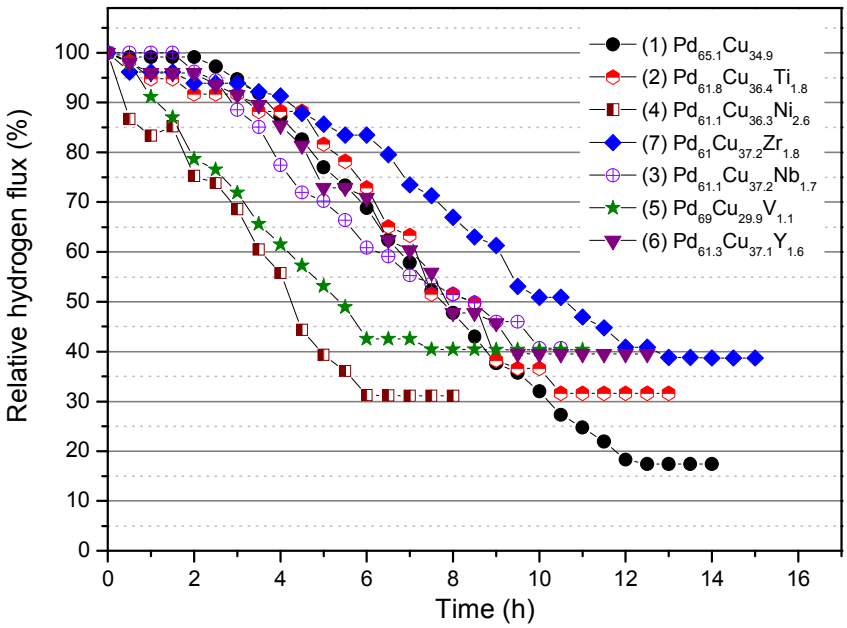

Figure 7: Sulphur poisoning of $Pd_{65.1}Cu_{34.9}$ and Pd–Cu–M (M= Y, Ti, Zr, V, Nb, and Ni) alloys at 450 °C. The feed gas contains 1000 ppm H_2S+H_2.

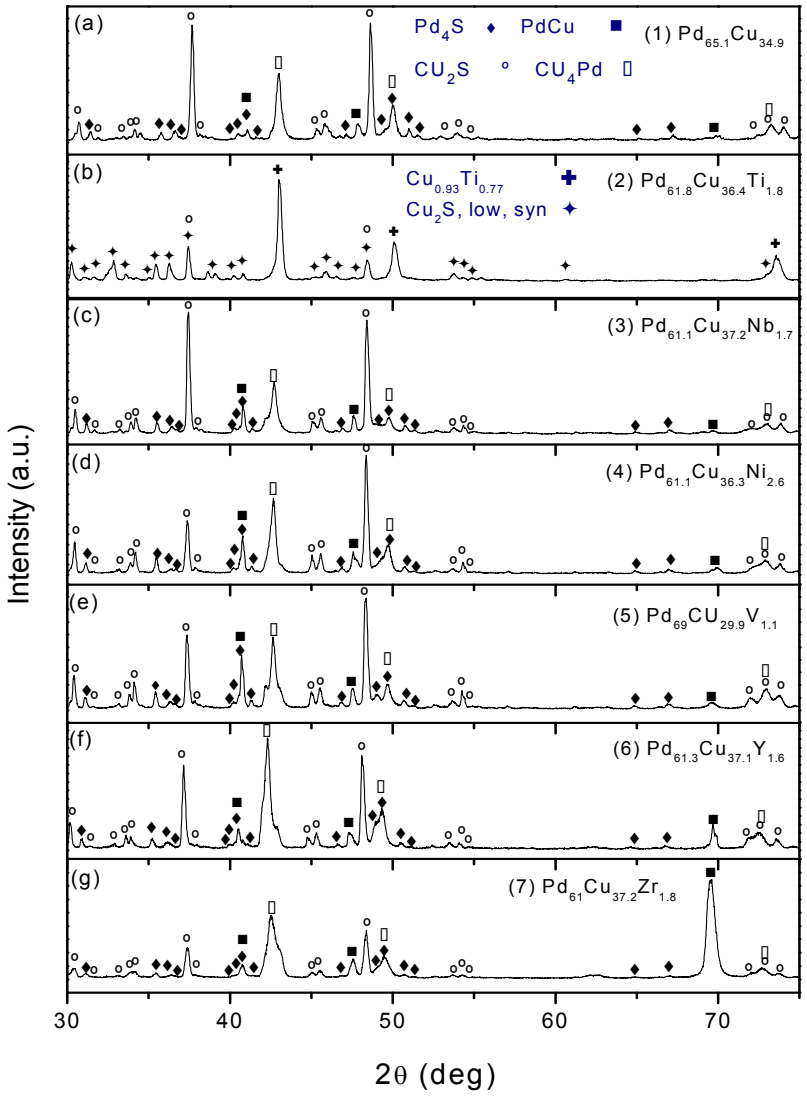

Figure 8: XRD patterns of (a) $Pd_{65.1}Cu_{34.9}$ and Pd–Cu–M alloys with (b) Ti, (c) Nb, (d) Ni, (e) V, (f) Y, and (g) Zr additional elements after exposure to 1000 ppm H_2S+H_2 at 450 °C.

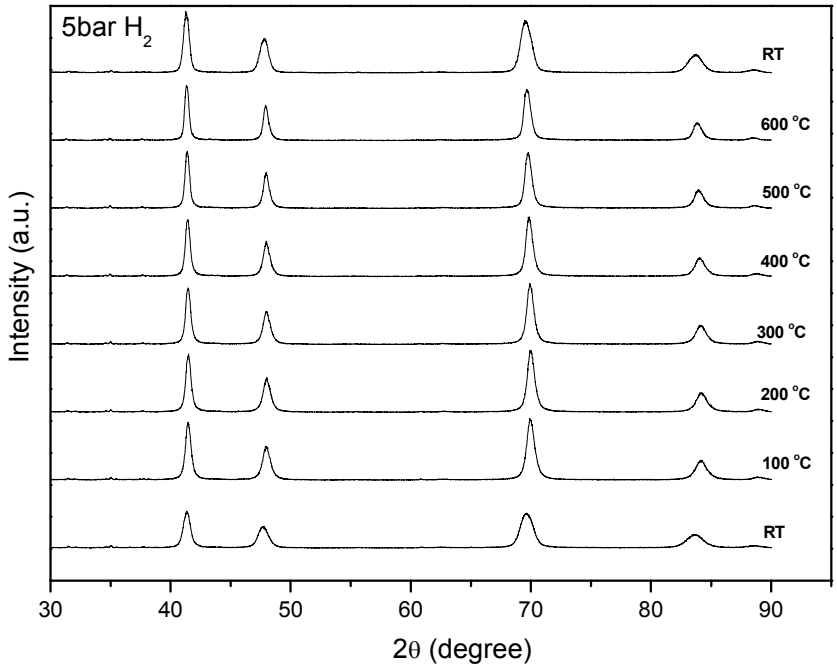

Figure 9: Evolution of the *in-situ* XRD patterns for Pd–Cu–Zr alloy under 5 bar hydrogen pressure. XRD patterns were collected at room temperature and the subsequent 100 °C increment steps to 600 °C, where the samples was cooled down to the room temperature before collecting the final XRD pattern.

Tables:

Table 1: EDS analyses of the $Pd_{65.1}Cu_{34.9}$ and Pd–Cu–M (M= Y, Ti, Zr, V, Nb, and Ni) alloys annealed at 650 ºC for 96 h. Also, atomic radii [43], valence [44], enthalpy for M–H formation [45], and foils thicknesses are included.

Sample	EDS (at%)			Atomic radius of M (Å)	Effective valence of M	Enthalpy of M-H formation (kJ/g atom)	Foil thickness (μm)	alloy phase
	Pd	Cu	M					
(1) PdCu	65.1±0.1	34.9±0.1	-	Pd:1.40 Cu:1.35	Cu:1		97	fcc
(2) PdCuTi	61.8±0.2	36.4±0.4	1.8±0.3	1.40	4	-42	91.4	fcc
(3) PdCuNb	61.1±0.6	37.2±0.6	1.7±0.1	1.45	5	-20	113	fcc
(4) PdCuNi	61.1±0.5	36.3±0.5	2.6±0.2	1.35	4	-1	83	fcc
(5) PdCuV	69±0.4	29.9±0.3	1.1±0.4	1.35	5	-18	98	fcc
(6) PdCuY	61.3±0.5	37.1±0.4	1.6±0.3	1.80	3	-72	123	fcc
(7) PdCuZr	61±0.4	37.2±0.5	1.8±0.4	1.55	4	-55	112.5	fcc

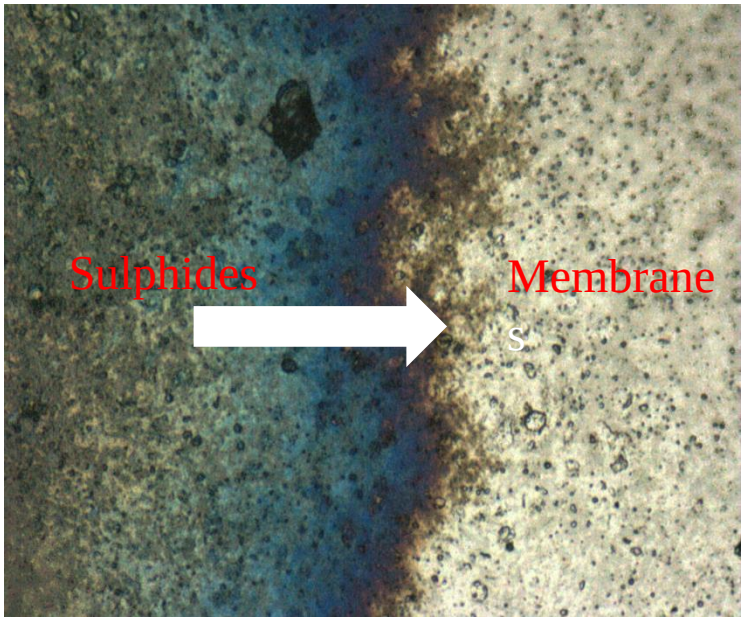

Progressive formation of sulphides on the surface of membrane